

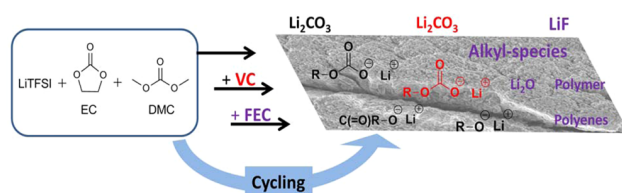
Surface Analytical Study Regarding the Solid Electrolyte Interphase Composition of Nanoparticulate SnO₂ Anodes for Li-Ion Batteries

V. Winkler,^{*,†,§,||} G. Kilibarda,^{†,§,⊥} S. Schlabach,[†] D. V. Szabó,[†] T. Hanemann,^{†,§} and M. Bruns^{†,‡}

[†]Institute for Applied Materials, and [‡]Karlsruhe Nano Micro Facility, Karlsruhe Institute of Technology, Hermann von Helmholtz Platz 1, 76344 Eggenstein Leopoldshafen, Germany

[§]Department of Microsystems Engineering, University of Freiburg, Georges Köhler Allee 102, 79110 Freiburg, Germany

ABSTRACT: This work presents a comparative surface analytical study on the solid electrolyte interphase (SEI) composition influenced by additives in the electrolyte using nanoparticulate SnO₂ as anode active material for lithium ion batteries (LIBs). In particular, lithium bis(trifluoromethanesulfonyl)imide (LiTFSI) based electrolytes in combination with vinylene carbonate (VC) and 1 fluoroethylene carbonate (FEC) as electrolyte additives are used. The SEI composition of the electrodes is investigated at two different aging stages by means of the complementary X ray photoelectron spectroscopy (XPS) and time of flight secondary ion mass spectrometry (ToF SIMS), providing chemical and molecular information on the topmost surface layers. We are able to show that the additives evolve different influences on the chemical composition of the formed SEI. The use of both additives generally results in an improved cycling stability of the nanoparticulate SnO₂ anodes. In consequence, these results open an effective possibility to improve the cycling stability of SnO₂ based electrode materials for LIBs by defined tailoring of the electrolyte's SEI composition.



1. INTRODUCTION

Today's state of the art lithium ion batteries (LIBs) are the leading and most valuable energy storage systems for mobile electronic devices like cell phones, laptops, and power tools due to their comparatively high energy density.¹⁻³ During the past decade, LIBs also gained more attention in the field of electrical vehicles. Therefore, the increasing demand for LIBs drives the worldwide development aiming at LIBs with high specific capacity and energy density to enable electrical vehicles with larger ranges that make them more attractive to the consumer market.⁴ To fulfill these central requirements for LIBs, several approaches at cell level like the development of new high voltage cathode or anode materials with improved specific capacities^{5,6} are currently in the focus of numerous R&D activities.^{1,7}

Materials based on silicon or tin have distinctively higher theoretical specific capacities (>700 mAh/g) as compared to the state of the art graphite anodes (372 mAh/g), and therefore are currently in the focus of research studies for anode materials.^{8,9} Whereas graphite acts as an intercalation host material with a rather low volume expansion (~10%) during cycling, the principle of anode materials based on silicon or tin is based on an alloying mechanism allowing one to store overall more lithium per atom of the active material but with the drawback of huge volume changes of up to 400% during lithiation and delithiation.^{10,11} Consequently, these volume changes will cause several problems like crack formation within the active material layer or contact loss toward the current collector during prolonged cycling.^{11,12} Additionally, the

inevitable pulverization of the active material leads to an exposure of nonpassivated active material during cycling. This will cause a continuous electrolyte degradation leading to an ongoing SEI building process, which ends up with an unfavorable capacity fading of such materials. These negative effects clearly are exclusion criteria for industrial applications. To encounter these problems, different approaches are discussed in the literature. One way is to stabilize the active material against extensive volume expansion either by synthesizing composite active material compounds^{13,14} or by using nanostructured active material.^{15,16} Another more cost effective approach is the usage of electrolyte additives, which are able to stabilize the SEI and reduce capacity fading during long term cycling. Here, vinylene carbonate (VC) and 1 fluoroethylene carbonate (FEC) are very prominent additives, which lead to a more favorable SEI composition. Both additives already proved their beneficial effect to enhance the cycling performance of silicon or tin based anodes.^{17,18} Because of the very different lithiation/delithiation process for alloying materials like silicon or tin as compared to the process of intercalation host materials, the SEI formation can deviate from already stated mechanisms valid for well known anode materials like graphite. Additionally, the SEI properties and therefore the overall performance as well as the long term stability of LIBs are also highly dependent on the electrolyte's

composition and interaction with the active material surface. To understand the relevant SEI building mechanisms while using alloying materials, it is important to investigate the chemical composition of the SEI.^{19–22}

In our previous work, we evidenced a significant improvement of the electrochemical performance of tin based nano composite electrodes adding 10% VC as additive to the electrolyte.²³ These experiments showed a simple way of optimizing the SEI properties by tailoring the electrolyte composition. The reason for the optimized performance has not been fully clarified yet. On the basis of these earlier results, we here focus on a comprehensive surface analytical characterization to elucidate a more detailed view on the influence of FEC and VC as very promising additives in the field of SnO₂ nanoparticle layered anode materials. In particular, complementary X ray photoelectron spectroscopy (XPS) and time of flight secondary ion mass spectrometry (ToF SIMS) were used to determine the chemical and molecular composition of the SEI on the surface and in depth to evaluate relevant SEI building processes. Additional information on the electrode's topography was achieved by means of scanning electron microscopy (SEM).

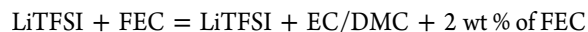
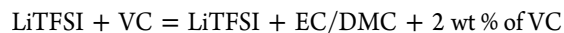
2. EXPERIMENTAL SECTION

Electrode Synthesis. Nanoparticulate SnO₂ thin films electrodes were synthesized using a microwave plasma process avoiding conventional slurry formation. The gas phase process for the synthesis of nanoparticles²⁴ uses water free tetra *n* butyltin, Sn(C₄H₉)₄ (ABCR, Karlsruhe, Germany), as precursor for the SnO₂ nanoparticles. A feeding rate of 5 ml h⁻¹ was selected. The reaction gas was a mixture of 80 vol % Ar + 20 vol % O₂ with a gas flow rate of 5 l min⁻¹. The power of the 2.45 GHz microwave was set to 600 W. These synthesis parameters have been selected, so that a SnO₂ nanoparticle layer thickness of around 2 μm was yielded in all cases. Furthermore, these special conditions enabled the synthesis of SnO₂ nanoparticles, in situ coated with a thin layer of hydrocarbons, C_xH_y, stemming from the organometallic precursor and adsorbed on the nanoparticles surface, necessary for electrical conductivity. Details about in situ hydrocarbon coating of Sn, respectively, SnO₂ nanoparticles, and characterization of the hydrocarbons with elemental analysis are described in our recently published work.^{23,24,29}

The resulting nanoparticles from the process were deposited in situ as porous films on 300 °C preheated Ni substrates according to the method described in previous studies.²⁴ These films were dried in a vacuum oven (Vacucenter VC20, Salvis Lab, Rotkreuz, Germany) for 2 h at 140 °C.

Cell Assembling and Electrolyte Composition. For cell cycling, SnO₂ half cells of Swagelok type were built up by using lithium foil (Alfa Aesar, Ward Hill, U.S.) as the counter and reference electrode. The cells were assembled in an argon filled Unilab glovebox (MBraun, Garching, Germany). Celgard 2325 (wetted in electrolyte overnight) was used as separator. The electrolyte consisted of a solution of 1 M LiTFSI (99.5%, trace metal basis, Sigma Aldrich) in ethylene carbonate (EC) and dimethyl carbonate (DMC) (50:50). Both additives, 1 fluoroethylene carbonate (FEC, 99%, Sigma Aldrich) and vinylene carbonate (VC, 99%, battery grade, 80 ppm BHT stabilized, Sigma Aldrich, activated by filtering over Al₂O₃), were used in a concentration of 2 wt %, respectively.

The following electrolyte compositions were tested:



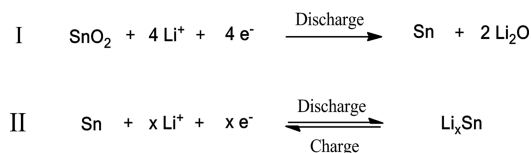
In contrast to our previous study on nanoparticulate Sn anodes,²³ we have chosen LiTFSI as salt instead of LiPF₆ because of its superior thermal stability and enhanced stability against moisture and decomposition especially in terms of long term cycling. It is therefore representing a promising salt for future applications in more stable electrolytes.^{25–27} Nevertheless, the relevant properties, conductivity and solubility of LiTFSI in EC/DMC, are comparable to LiPF₆, and therefore LiTFSI based electrolytes are expected to reveal results similar to those of commonly used LiPF₆ based electrolytes.^{27,28} Hence, the major SEI building processes in DMC and EC solvents are not significantly influenced by the exchange of the used conducting salt.

Electrochemical Characterization. Battery cycling was done using a lithium cell cyler (LICCY, developed at Karlsruhe Institute of Technology, Institute for Data Processing and Electronics, Germany) and a VMP3 multichannel potentiostat (Bio Logic, France).

The SnO₂ anodes were cycled in the voltage range of 0.1–2.8 V at a constant current rate corresponding to a C rate of C20. The corresponding current was calculated according to the active material weight directly yielded from the synthesis by weighting the substrates. Cells cycled for 3 cycles were regarded as “initial”, and cells cycled for in total 30 cycles were considered as “aged”.

In the present study, cell cycling at higher currents was omitted, due to the previously shown dramatic increase of the degradation of the active material.²⁹ Scheme 1 shows the present electrode reactions taking place during charging and discharging of SnO₂. According to the literature, during the first discharging cycle of SnO₂ anodes, metallic tin and lithium oxide are formed within an irreversible reaction (Scheme 1, reaction I).^{30,31} Subsequent charging and discharging is based on a reversible lithiation/delithiation reaction in kind of alloying/dealloying of tin (Scheme 1, reaction II).^{30,31} The disassembling of the cells was performed in the delithiated state of the electrodes.

Scheme 1. Irreversible Reaction of SnO₂ Anode Material during the First Discharging Cycle (I) and Reversible Lithiation and Delithiation Reaction during Ongoing Cycling (II)



After cell cycling, all three surface analysis methods (XPS, ToF SIMS, and SEM) were performed consecutively on each sample, providing complementary information. Prior to the characterization, all cycled samples were carefully rinsed using a mixture of DMC and 5 vol % propylene carbonate (PC, 99%, Sigma Aldrich) immediately after cell disassembling inside the glovebox.

XPS Characterization. The XPS measurements were performed using a K Alpha XPS spectrometer (Thermo Fisher

Scientific, East Grinstead, UK). Data acquisition and processing using the Thermo Avantage software is described elsewhere.³² All samples were analyzed using a microfocused, monochromated Al K_{α} X ray source (400 μm spot size). The acquired spectra were fitted with one or more Voigt profiles (binding energy uncertainty: ± 0.2 eV). The analyzer transmission function, Scofield sensitivity factors,³³ and effective attenuation lengths (EALs) of photoelectrons were applied for quantification. EALs were calculated using the standard TPP 2M formalism.³⁴ All spectra were referenced to the C 1s peak of hydrocarbon at 285.0 eV binding energy controlled by means of the well known photoelectron peaks of metallic Cu, Ag, and Au. Sputter depth profiles were performed using a raster scanned Ar^+ ion beam at 0.5 keV and 30° angle of incidence. For sample handling and transfer without atmospheric contact, an Ar glovebox is directly attached to the loadlock of the K Alpha.

ToF-SIMS. Time of flight secondary ion mass spectrometry was performed on a TOF SIMS 5 instrument (ION TOF GmbH, Münster, Germany), equipped with a Bi cluster liquid metal primary ion source and a nonlinear time of flight analyzer. The Bi source was operated in the “bunched” mode providing 1 ns Bi_3^+ ion pulses at 25 keV energy, an analyzed area of $128 \times 128 \mu\text{m}^2$, and a lateral resolution of approximately 4 μm . Sputter depth profiles were performed using a 1 keV Cs^+ ion beam and a raster size of $500 \times 500 \mu\text{m}^2$. For all secondary ion images, the first 20 scans (x - y plane) within a recorded sputter depth profile using Cs ions, equivalent to 100 s etching time, were summed.

Positive polarity spectra were calibrated on the ${}^6\text{Li}^+$, C^+ , CH^+ , CH_2^+ , and CH_3^+ , C_2H_5^+ , Cs_2^+ peaks. All samples were transferred via a hermetically sealed transfer vessel customized by ION TOF; sample handling was performed within the K Alpha glovebox system.

SEM. SEM images were recorded with a Zeiss Merlin scanning electron microscope (Carl Zeiss SMT AG, Oberkochen, Germany), equipped with a Schottky field emission source (acceleration voltage of 2 kV within the in lens mode, otherwise 10 kV). Sample transport from the K Alpha glovebox to the microscope was achieved by a specially designed inert gas transport vessel via flange connections.

3. RESULTS AND DISCUSSION

Regarding the electrochemical results of the galvanostatic cycling, the three used electrolytes revealed significant differences in the overall cycling performance (Figure 1). The best results with respect to cycling stability were achieved when using FEC as additive within the electrolyte (Figure 1, blue curves). Also, with the VC containing electrolyte (Figure 1, red curves), it was possible to enhance the cycling performance as compared to the pure LiTFSI based electrolyte (Figure 1, black curves).

For all three electrolytes, it takes at least three cycles until the Coulombic efficiencies (CE) are beyond 90% and stabilized cycling performances were reached. The poor CE during the initial cycling is mainly due to the SEI formation. Note that the unusual high specific capacity of the first cycles, respectively, is not only ascribed to the SEI formation. It also refers to an additional contribution of hydrocarbons with a high H/C atomic ratio to the specific capacity. The same effect was also discussed in detail in our previously published work and can be confirmed by other research studies found in the literature.^{23,35,36} Once a stable SEI passivation layer is formed,

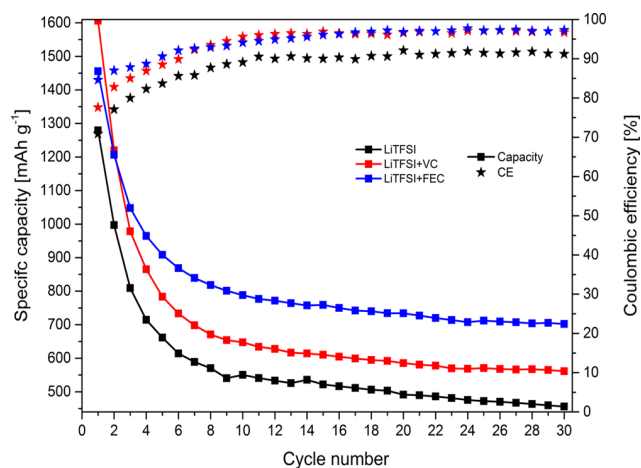


Figure 1. Specific discharge capacities and Coulombic efficiencies (CE) of nanoparticulate SnO_2 electrodes (vs Li^+) cycled in LiTFSI, LiTFSI+VC, and LiTFSI+FEC electrolyte, respectively.

further parasitic electrolyte decomposition on top of the electrode surface is prevented. Accordingly, the CE increases for all investigated electrolytes. Nevertheless, during consecutive cycling, a still ongoing degradation for all electrodes is detectable. This is mainly related to the formation of cracks within the active material layer caused by the volume expansion during lithiation/delithiation. The crack formation will lead to an exposure of fresh active material sites toward the electrolyte resulting in a further SEI buildup. Figure 2 shows exemplarily the

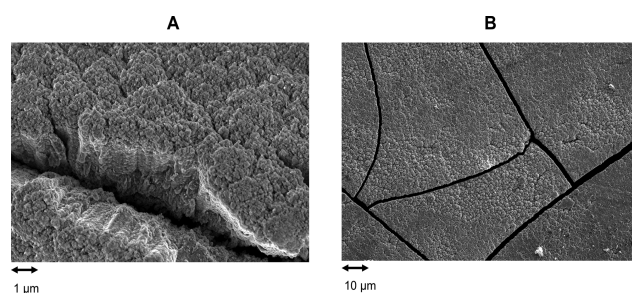


Figure 2. SEM images of a pristine nanoparticulate SnO_2 electrode (A) and an initially cycled electrode in LiTFSI (B). The columnar electrode structure (A) and the crack forming caused by the volume expansion during cycling (B) are illustrated.

crack formation for the electrode cycled in LiTFSI electrolyte as compared to a pristine electrode surface. With only minor differences, this crack forming process was observable for all electrodes and is independent from the used electrolyte (cf., Figure S4). Such a crack formation was also observed in our previous studies.²³ We therefore conclude that the observed differences in the cycling behavior of the three compared electrolytes must be related to another mechanism. Anyway, FEC as well as VC containing electrolytes delivered a more effective SEI formation and therefore an improved cycling performance as compared to the additive free LiTFSI electrolyte. However, only a systematic investigation of the SEI composition using surface analytical methods will allow for a better understanding of the underlying mechanisms and gaining deeper insights into the interaction between the active material and electrolyte.

3.1. Composition of the SEI Determined by XPS.
3.1.1. Additive-Free LiTFSI-Based Electrolyte. Figure 3 compares the XPS results of the three initial cycled electrodes

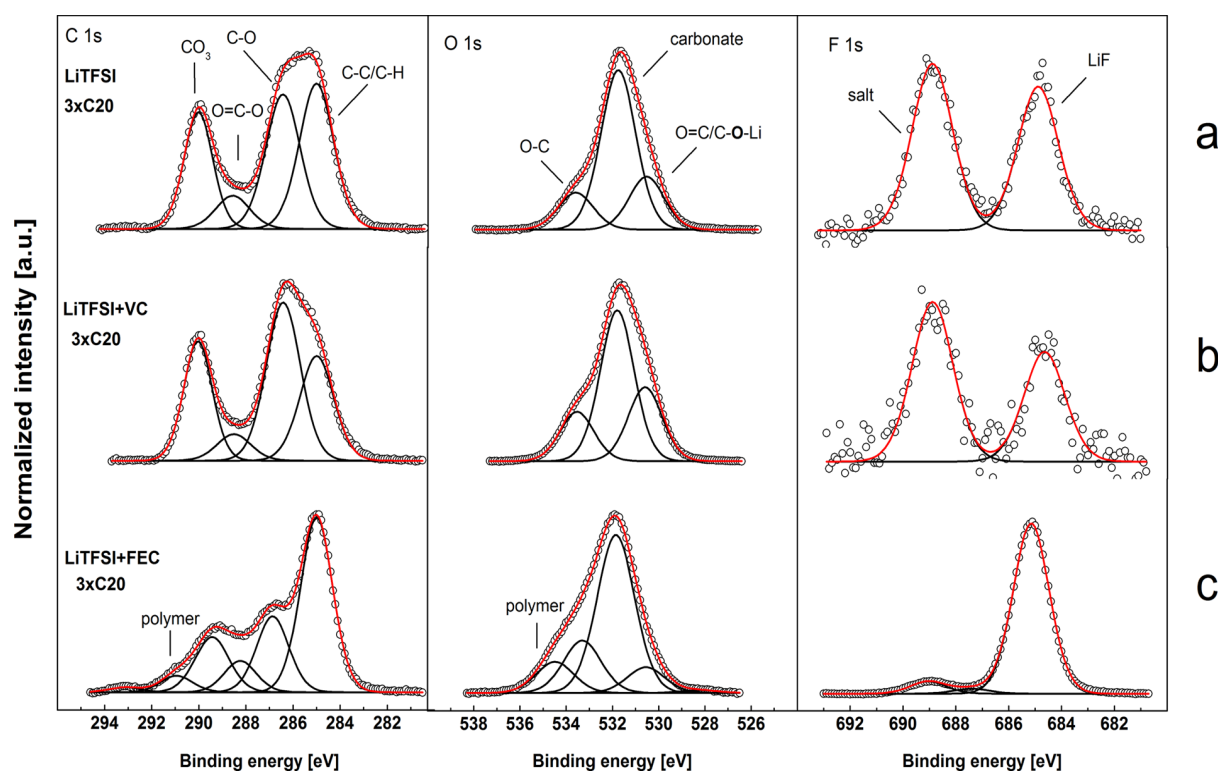


Figure 3. C 1s, O 1s, and F 1s XP spectra of nanoparticulate SnO₂ electrode surfaces after initial cell cycling (3 cycles at C20) using LiTFSI (a), LiTFSI+VC (b), or LiTFSI+FEC (c).

Table 1. XPS Binding Energies with Assignments and the Corresponding Atomic Concentrations of the Identified Components of All Nanoparticulate SnO₂ Anodes Cycled in LiTFSI Based Electrolytes

photoelectron peak	BE [eV]	concentration [at. %]						assignment
		LiTFSI		LiTFSI+VC		LiTFSI+FEC		
		3 × C20	30 × C20	3 × C20	30 × C20	3 × C20	30 × C20	
Li 1s	53.9					3.4	4.5	Li ₂ O
Li 1s	55.7	27.7	26.5	27.9	28.2	27.9	24.5	Li ⁺
S 2p _{3/2}	169.1					0.5	0.4	salt
C 1s	285.0	10.8	9.0	8.2	10.8	11.8	13.3	C C/C H
C 1s	286.9	9.9	12.8	12.4	11.3	5.2	6.2	C O
C 1s	288.2	2.5	3.0	2.1	1.9	2.1	2.6	O C O
C 1s	289.4	7.2	7.6	7.8	7.6	4.0	4.2	O C(O) O
C 1s	290.9					1.1	1.5	polymer
C 1s	293.1					0.3	0.2	salt
N 1s	399.9					0.5	0.3	salt
Sn 3d _{5/2}	483.4	0.3	0.1	0.2	0.2	0.1	0.1	Li _x Sn
Sn 3d _{5/2}	486.9	0.4	0.2	0.1	0.1	0.2	0.3	SnO ₂
O 1s	528.2					0.6	0.7	Li ₂ O
O 1s	530.6	8.4	6.5	11.0	9.7	2.1	1.9	O C/C O Li
O 1s	531.9	25.4	25.8	22.4	21.6	12.7	10.9	CO ₃ (carbonate)
O 1s	533.3	5.9	7.5	7.3	7.2	4.2	5.7	O C
O 1s	534.5					2.5	3.4	polymer
F 1s	685.2	0.7	0.3	0.2	0.3	19.2	16.9	LiF
F 1s	687.4					0.6	1.1	salt-decomp
F 1s	689.0	0.8	0.7	0.4	0.5	1.4	1.3	salt

using the respective electrolytes. The results of the samples cycled either in LiTFSI, LiTFSI+VC, or LiTFSI+FEC are discussed in the appropriate subsections. Figure 3a shows the C 1s, O 1s, and F 1s XP spectra of the sample initially cycled for 3 cycles with C20 using the additive free LiTFSI based electrolyte. The corresponding assignments and quantification of the fitted components are compiled in Table 1. The binding

energies in the C 1s spectrum of 285.0 eV (C–C/C–H), 286.9 eV (C–O), 288.2 eV (O=C–O), and 289.4 eV (O–C(=O)–O) correspond well to the findings in the O 1s spectrum at binding energies of 530.6 eV (O=C/C–O–Li), 531.9 eV (O–C(=O)–O), and 533.3 eV (C–O) and confirm the incorporation of a mixture of several organic and inorganic compounds like carbonates, semi

carbonates, esters, and ethers into the SEI layer.^{37–40} These compounds can be ascribed to the decomposition of EC and DMC during the first cycles.

In contrast to cycled graphite anodes under similar conditions,⁴¹ the overall amount of oxidized carbon species and the ratio of the carbonate component normalized to the C–O component within the SEI layer are comparatively high in the nanoparticulate SnO₂ electrode samples. This demonstrates the more inorganic nature of the formed carbonates (i.e., Li₂CO₃) and is corroborated by the absence of C–O bonds expected for products based on esterification of organic carbonates or semicarbonates. Likewise, the total lithium content of 27.7 at. % related to lithium containing SEI compounds like Li₂CO₃ is comparatively high, too. Especially in the first cycles, irreversible reactions between the solvents and lithium occur forming the SEI layer. This irreversible consumption of lithium for SEI forming is the main reason for the high current loss resulting in lower Coulombic efficiencies (Figure 1, black curve). As all samples were disassembled in the delithiated state of the electrode and only minor unreacted lithiated tin species could be detected, all identified lithium species can be assigned to SEI compounds. Both the high amount of oxidized carbon species and the high lithium content within the SEI are very likely originated by the high reactivity of the nanoparticle layered SnO₂ anode surface causing an accelerated decomposition of the electrolyte solvents.

In contrast, the F 1s spectrum indicates a low content of fluorine species like LiF (F 1s = 685.2 eV)⁴⁰ besides small amounts of conductive salt residues. This finding proves the stability of LiTFSI against decomposition during cycling despite a highly reactive SnO₂ surface. However, after 3 cycles, the nanoparticulate SnO₂ thin film anode shows already a distinctive crack formation within the columnar morphology (Figure 2b), which couldn't be prevented by the present SEI layer. The crack formation is caused by the dramatic volume expansion of the active material during the lithiation/delithiation process and is well described in the literature.^{19,20} These cracks in addition might be the reason for the fact that lithiated and unreacted tin species are still detectable in small amounts even after three cycles, although the average SEI thickness is expected to be already thicker than the XPS sampling depth (~5–8 nm).²⁹

The XP spectra of the aged cell basically show the same features as compared to the spectra of the initial cycled cell. However, the ratios of oxidized carbon components referred to the alkyl component (C–C/C–H) at 285.0 eV binding energy are slightly increased (Figure S1a). In parallel, the ratios between the single oxidized carbon components stayed nearly constant. These effects can be explained by a growth of the SEI layer during cycling due to the further decomposition of carbonate solvents. A detailed analysis of the quantified amounts additionally reveals an enhanced ratio of the C–O content as compared to the other species and is reflected by the increased peaks in the carbon spectrum at 286.9 eV as well as in the oxygen spectrum at a binding energy of 533.3 eV. The assignments and quantification of the fitted components are summarized in Table 1.

Despite the mentioned minor changes of the SEI layer during cycling, the SEI and its main components preserved roughly their initial composition. This is supported by the trend of the Coulombic efficiency (CE, Figure 1, black curve) during cycling. Only the first initial cycles show a lower CE due to

current losses related to the SEI building process. With ongoing cycling, the CE immediately begins to increase showing a stabilization of the SEI layer with only minor losses due to parasitic side reactions. Finally, the stability of the LiTFSI salt during cycling is evidenced by the very small amount of its decomposition products within the SEI, indicated by the low content of fluorine compounds even after 30 cycles.

3.1.2. LiTFSI-Based Electrolyte Containing VC as Additive. The reason for using VC as additive in the electrolyte is to achieve a flexible SEI layer to improve the mechanical as well as the electrochemical properties of the SEI, for example, by integrating polymer like species into the surface layer via the polymerization of VC.³³ Such polymerization should already be initialized at lower reduction potentials during the first discharge cycle and, therefore, prior to any decomposition reaction of DMC or EC.^{20,21}

However, the XP spectra of the SnO₂ samples cycled in the VC containing electrolyte reveal no distinctive changes in the SEI composition as compared to samples cycled in pure LiTFSI electrolyte (Figure 3b). Although an increased ratio of the oxidized carbon species (C 1s = 286.9 eV (C–O), 288.2 eV (O=C–O), and 289.4 eV (O–C(=O)O) toward the alkyl component at 285.0 eV (C–C/C–H) is visible (cf., Table 1), no significant features representing a polymer like species or distinctive features of VC can be identified. Furthermore, the rise of the oxygen species at 530.6 eV assigned to lithiated alkoxy compounds is more related to decomposition products of DMC or EC than VC. The content of lithium species is comparable to samples cycled in pure LiTFSI electrolyte. In conclusion, the VC additive unexpectedly does not affect the composition of the SEI on nanoparticulate SnO₂ anodes that strong. The XPS results differ from those of our previous investigation on similar tin based anodes,²³ where we have used 10 wt % VC within the electrolyte mixture and LiPF₆ as salt. The results are also in contrast to the known behavior of graphite electrodes.^{41,42} The mechanisms discussed in the literature are obviously not the only key to fully stabilize the SEI layer and thus increase the performance of nanoparticulate SnO₂ anodes.^{20,21} Nevertheless, an improvement of the cycling behavior can be achieved already with a small percentage of VC (cf., Figure 1, red curve). Therefore, we suggest that the predominant solvent decomposition reactions observed in the present study can be encountered by raising the additive content yielding a favored incorporation of VC products into the SEI, finally leading to an overall stabilization of the passivation layer. In conclusion, the present SEI layer is predominantly consisting of SEI species related to the decomposition of the main electrolyte solvent components EC and DMC. This is obviously linked to the high reactivity of the nanoparticulate SnO₂ electrode surface, which favors the decomposition of the main electrolyte components within the SEI building process. These major decomposition products of EC and DMC likely superimpose small amounts of VC related SEI species, which complicates the clear identification of the latter by XPS.

No major differences in the XP spectra of the initial cycled electrode and the aged electrodes are found in the case of LiTFSI+VC electrolyte (cf., Figure S1b and Table 1). This is similar to the samples cycled in pure LiTFSI electrolyte. Although there is an increase of the alkyl component as compared to the oxidized carbon species, the ratios between these single oxidized species stayed the same, indicating a similar nature of the respective SEI compounds. In conclusion,

the SEI composition does not change significantly during prolonged cycling. Also, the LiTFSI salt stays stable within the performed cycling tests, indicated by still small amounts of fluorine species. Despite small differences in the SEI composition when using VC as additive as compared to the pure LiTFSI electrolyte, the electrochemical performance and cycling stability can be increased (Figure 1, red curve), proving a beneficial effect even at small additive concentrations. This also supports the assumption that SEI products of VC are superimposed by the predominant solvent decomposition products of EC and DMC, which complicates the identification by XPS.

3.1.3. LiTFSI-Based Electrolyte Containing FEC as Additive.

The second very promising additive in the present study is FEC, aiming again at the improvement of the SEI properties and, therefore, the overall electrochemical performance especially regarding the long term stability.^{43,44} For active materials like silicon oxide, improved cycling stability is already agreed upon in the literature but is not as well understood as compared to the mechanisms accompanying/incorporating VC.^{45,46} Moreover, in our study, FEC can solve the problem of missing fluorine species when using LiTFSI based electrolytes. Because the LiTFSI salt is more stable in contrast to LiPF₆, a lack of fluorine species can cause a less stable SEI layer and will also lead to corrosion of the aluminum current collector on the cathode side.²⁶ Using FEC, a sufficient amount of fluorine via an electrochemical induced defluorination reaction of the molecule during cycling can be expected enabling us to circumvent the above mentioned problems.

The XP spectra (Figure 3c) of the initial cycled sample in LiTFSI+FEC directly prove the distinctive influence of FEC on the SEI building process. The C 1s spectrum reveals significantly lower amounts of oxidized carbon species especially for the carbonate component at 289.4 eV and C–O species at 286.9 eV binding energy. The corresponding quantitative amounts of O 1s components at binding energies of 531.9 eV (CO₃) and 533.3 eV (C–O) corroborate these findings (cf., Table 1). The new component at C 1s = 290.9 eV and O 1s = 534.5 eV, respectively, is attributed to polymer species originating from FEC. This assignment is directly justified by the results of our synthesized VC reference polymer (C 1s = 288.1 and 291.4 eV, O 1s = 533.1 and 535.0 eV) and in very good agreement with literature data.⁴² Figure 4 (top)

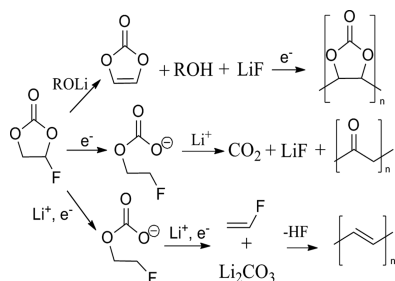


Figure 4. Possible decomposition pathways of FEC.^{43,45,47}

displays a potential decomposition path for FEC leading to VC as an intermediate and finally to a polycarbonate polymer species.⁴³ However, the comparatively small amount of the assigned polymer species and high content of C–C/C–H carbon require an additional organic species. In consequence, an alternative FEC decomposition pathway, like the formation of an olefinic polymer species (Figure 4, bottom),⁴⁷ seems to be

favored when using a highly surface reactive electrode substrate like the present nanoparticulate SnO₂.

The amount of LiF (F 1s = 685.2 eV) clearly evidenced the expected capability of FEC to provide fluorine necessary for stabilizing the SEI and enabling the corrosion protection of the current collector (cf., Table 1).⁴⁷ The overall lithium content of about 27.9 at. % is comparable to the other samples cycled in LiTFSI based electrolytes. Yet the Li 1s peak now has a pronounced asymmetric tailing at lower binding energies (see Figure S3). Corresponding with a new O 1s peak at 528.2 eV, we assume the formation of Li₂O.⁴⁸ A possible origin for Li₂O is the decomposition of already existing SEI species like Li₂CO₃, but also species out of the irreversible reaction step during the first discharge cycle (Scheme 1, reaction I) cannot be excluded. The clarification of the real origin of Li₂O and why it is exclusively seen when using the LiTFSI+FEC electrolyte remains an open question.

As for all other tested LiTFSI based electrolyte compositions, also for the FEC additive based electrolyte no major effects toward the SEI composition arise from the applied aging procedure (Figure S1c). In accordance with the aged samples of the other two electrolytes, only minor further electrolyte decomposition takes place. Still the total amount of oxidized carbon species is reduced when using FEC, while the alkyl component is the dominant species in the C 1s spectrum. The further increase of the Li₂O amount during aging might originate from still ongoing decomposition reactions of already existing SEI compounds like Li₂CO₃ in agreement with the reduced amount of carbonate species as compared to the other electrolytes.

The associated XPS sputter depth profile of the aged sample (Figure S2) evidenced a constant amount of the fluorine species across the SEI. This proves that the fluorine release of FEC is homogeneously distributed all over the SEI layer thickness and not only located close to the active material site. Finally, when comparing the XPS results of the electrolytes containing FEC or VC, it is evident that spectra from FEC electrolytes show clearly more pronounced features of additive related decomposition products than spectra from VC electrolytes. This shows the greater influence of FEC on the overall SEI composition. Consequently, the underlying decomposition processes must be different for both additives with more advantageous cell performance in the case of FEC. A reasonable explanation is that FEC exhibits faster decomposition kinetics than VC. This mechanism is even more important in the case of highly surface reactive active materials like the present nanoparticulate SnO₂.

In conclusion, using FEC as an electrolyte additive shows the most positive influence on the cycling behavior (Figure 1). This can be observed for the initial discharge capacities and the Coulombic efficiencies as well as for the superior specific capacities of all tested electrolyte compositions. These enhanced cycling properties can be closely connected to the existence of the detected polymer and alkyl species within the SEI layer when using FEC. Because we did not notice major differences in the crack formation between the single samples (see Figure 2, Figures S3 and S4), we assume that the SEI has a more flexible nature, which stabilizes the passivation layer and minimizes further electrolyte decomposition as well as the loss of lithium due to parasitic reactions when using FEC.

Consequently, taking the discussed results of XPS into account and comparing all three electrolytes, the overall lower amount of oxidized carbon species can serve as a decisive factor

in evaluating the quality and electrochemical properties of the SEI.

3.2. Lateral and In-Depth Elemental Distribution Determined by ToF-SIMS. Especially for carbonate solvent based electrolytes and in the case of using VC or FEC as electrolyte additive, the 3D distribution of the carbonate SEI components is a key aspect in evaluating the forming processes and quality of the SEI. This aspect was investigated by means of ToF SIMS sputter depth profiling. The processes during SEI formation as well as the resulting basic SEI compounds identified with ToF SIMS were very similar for all investigated samples. Therefore, we discuss exemplarily the ToF SIMS data measured on the LiTFSI sample.

3.2.1. Initial SEI. Figure 5 shows the lateral and in depth distribution of carbonate compounds within the SEI layer using

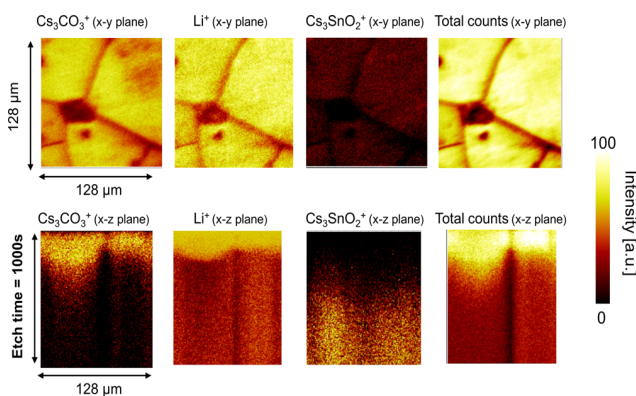


Figure 5. ToF SIMS images of an initially cycled nanoparticulate SnO₂ electrode (LiTFSI), showing the total ion count, Li⁺, and the positive secondary cluster ions Cs₃CO₃⁺ and Cs₃SnO₂⁺, each in the *x*-*y* plane (top) and *x*-*z* plane (bottom) view, respectively.

the Cs₃CO₃⁺ fragment as indicator. The lateral distribution of the carbonate as well as the lithium SEI species at the topmost surface of the SEI are homogeneous (Figure 5, top). Additionally, the cracks mentioned before, formed during the initial cycling (cf., Figure 2 and Figure S4), are clearly visible within the secondary ion image. A view along the *x*-*z* plane reveals the in depth distribution of carbonate and lithium containing SEI species, respectively (Figure 5, bottom). This clearly evidences an accumulation of the SEI species mainly at the topmost surface within a layer of about 10–15 nm thickness. In contrast, the Cs₃SnO₂⁺ secondary cluster ion is only detected in deeper layers. This corroborates the assumption that during the initial cycling the SEI formation on reactive surface sites is preferred.

3.2.2. Aged SEI. Figure 6 shows the ToF SIMS secondary ion images of Cs₃CO₃⁺, Li⁺, Cs₃SnO₂⁺, and the total ion intensity of the aged nanoparticulate SnO₂ sample. Similar to the initially cycled sample, the lateral distribution of the carbonate and lithium containing SEI species at the electrode surface is homogeneous. However, the *x*-*z* cross sectional views (Figure 6, bottom) doubtlessly prove the progress of the formation of these SEI species toward deeper layers. Again, we assume that at the beginning of the cell cycling, the carbonate species will be formed preferably at positions of highest reactivity located at the topmost surface. With ongoing cycling, this formation and the respective species will propagate into deeper layers of the SnO₂ electrode. In addition, the aged electrode shows a higher number of cracks of distinctively shorter lengths. This, in consequence, causes an increasing

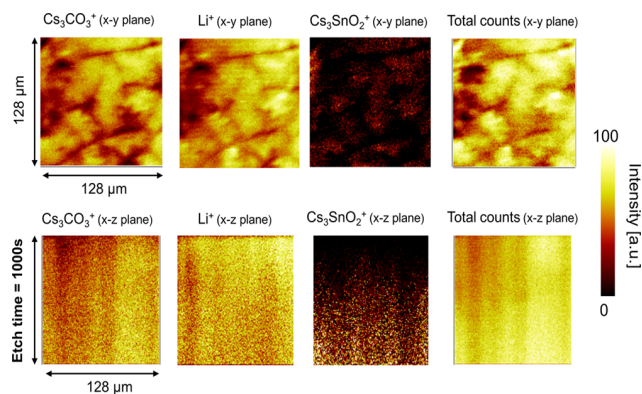


Figure 6. ToF SIMS images of an aged nanoparticulate SnO₂ electrode (LiTFSI), showing the total ion count, Li⁺, and the positive secondary cluster ions Cs₃CO₃⁺ and Cs₃SnO₂⁺ each in the *x*-*y* plane (top) and *x*-*z* plane (bottom).

quantity of pristine SnO₂ surfaces freshly exposed to the electrolyte resulting in a further SEI formation in conjunction with an ongoing decomposition of the electrolyte resulting in lower CE and continuous degradation of the electrodes (cf., Figure 1).

Because the ToF SIMS results were very similar for all electrodes cycled in the chosen electrolytes, the progress of the SEI formation and its development during aging differ only slightly. Nevertheless, XPS proved that the key issue for evaluating the properties of the SEI is to evaluate its chemical composition. When using active materials of high surface reactivity like nanoparticulate SnO₂ films, FEC is the additive of choice to improve the batteries properties. FEC containing electrolytes provide improved electrochemical performance as compared to pure or VC containing LiTFSI electrolytes even after aging. For an overview, Figure S5 gives a schematic summary of the identified SEI products using the respective electrolytes.

4. CONCLUSION

In this study, we have investigated the chemical composition of the SEI formed in LiTFSI based electrolytes using VC and FEC as performance improving additives for nanoparticulate SnO₂ film anodes. Using complementary XPS and ToF SIMS, we gained new insights in the SEI formation, and we were able to correlate electrochemical cycling performance data with the chemical composition of the SEI layer. Particularly, our study proved a high surface reactivity of nanoparticulate SnO₂ electrodes leading to a significant amount of oxidized carbon surface species, mainly Li₂CO₃, already after the initial cycling. The high surface reactivity of SnO₂ leads to a preferred decomposition of the main electrolyte components EC and DMC. This complicates the identification of VC related SEI species via XPS. Despite this, the FEC additive was able to influence the SEI composition more reasonably, resulting in a further improvement of the cycling properties as compared to the pure LiTFSI or LiTFSI+VC electrolyte. Therefore, we suggest a faster and favored decomposition reaction of FEC as compared to VC, leading to a more pronounced impact on the SEI properties. Nevertheless, both additives were able to improve the overall cycling performance of nanoparticulate SnO₂ electrodes showing their positive impact toward the SEI properties. Moreover, the combination of LiTFSI based electrolytes together with FEC shows a promising approach for an electrolyte mixture benefiting from a more thermic and

moisture stable salt as compared to LiPF_6 . Simultaneously, the discussed problems accompanying LiPF_6 like reduced/missing fluorine species and aluminum current collector corrosion are circumvented while using FEC as fluorine donating source in combination with LiTFSI. Additionally, ToF SIMS studies enable us to follow the lateral and in depth elemental distribution of SEI species. At the initial state of the SEI, a homogeneous distribution of SEI species concentrated at the electrode surfaces was evidenced. During ongoing cycling, the decomposition process of the electrolyte and the respective SEI species propagates into deeper layers depending on the aging state of the electrodes.

AUTHOR INFORMATION

Corresponding Author

*E mail: volkerwinkler@web.de.

Present Addresses

^{||}IPREM, Equipe Chimie Physique, UMR 5254 UPPA/CNRS, Technopole Helioparc, 2 avenue du President Angot, 64000 Pau, France.

[†]Varta Microbattery, Daimlerstraße 1, 73479 Ellwangen, Germany.

Notes

The authors declare no competing financial interest.

ACKNOWLEDGMENTS

We gratefully acknowledge the support of Udo Geckle for SEM analysis.

REFERENCES

- (1) Wagner, R.; Preschitschek, N.; Passerini, S.; Leker, J.; Winter, M. Current research trends and prospects among the various materials and designs used in lithium based batteries. *J. Appl. Electrochem.* **2013**, *43*, 481–496.
- (2) Marom, R.; Amalraj, S. F.; Leifer, N.; Jacob, D.; Aurbach, D. A review of advanced and practical lithium battery materials. *J. Mater. Chem.* **2011**, *21*, 9938–9954.
- (3) Scrosati, B.; Garche, J. Lithium batteries: Status, prospects and future. *J. Power Sources* **2010**, *195*, 2419–2430.
- (4) Goodenough, J. B.; Park, K. S. The Li Ion Rechargeable Battery: A Perspective. *J. Am. Chem. Soc.* **2013**, *135*, 1167–1176.
- (5) Patoux, S.; Daniel, L.; Bourbon, C.; Lignier, H.; Pagano, C.; Le Cras, F.; Jouanneau, S.; Martinet, S. High voltage spinel oxides for Li ion batteries: From the material research to the application. *J. Power Sources* **2009**, *189*, 344–352.
- (6) Xu, B.; Qian, D.; Wang, Z.; Meng, Y. S. Recent progress in cathode materials research for advanced lithium ion batteries. *Mater. Sci. Eng., R* **2012**, *73*, 51–65.
- (7) Zhang, W. J. A review of the electrochemical performance of alloy anodes for lithium ion batteries. *J. Power Sources* **2011**, *196*, 13–24.
- (8) Liang, B.; Liu, Y.; Xu, Y. Silicon based materials as high capacity anodes for next generation lithium ion batteries. *J. Power Sources* **2014**, *267*, 469–490.
- (9) Nitta, N.; Yushin, G. High Capacity Anode Materials for Lithium Ion Batteries: Choice of Elements and Structures for Active Particles. *Part. Part. Syst. Charact.* **2014**, *31*, 317–336.
- (10) Winter, M.; Besenhard, J. O. Electrochemical lithiation of tin and tin based intermetallics and composites. *Electrochim. Acta* **1999**, *45*, 31–50.
- (11) Park, C. M.; Kim, J. H.; Kim, H.; Sohn, H. J. Li alloy based anode materials for Li secondary batteries. *Chem. Soc. Rev.* **2010**, *39*, 3115–3141.
- (12) Chen, D.; Indris, S.; Schulz, M.; Gamer, B.; Mönig, R. In situ scanning electron microscopy on lithium ion battery electrodes using an ionic liquid. *J. Power Sources* **2011**, *196*, 6382–6387.
- (13) Wang, G.; Wang, B.; Wang, X.; Park, J.; Dou, S.; Ahn, H.; Kim, K. Sn/graphene nanocomposite with 3D architecture for enhanced reversible lithium storage in lithium ion batteries. *J. Mater. Chem.* **2009**, *19*, 8378–8384.
- (14) Hassoun, J.; Derrien, G.; Panero, S.; Scrosati, B. A Nano structured Sn–C Composite Lithium Battery Electrode with Unique Stability and High Electrochemical Performance. *Adv. Mater.* **2008**, *20*, 3169–3175.
- (15) Yang, Z.; Du, G.; Meng, Q.; Guo, Z.; Yu, X.; Chen, Z.; Guo, T.; Zeng, R. Dispersion of SnO_2 nanocrystals on $\text{TiO}_2(\text{B})$ nanowires as anode material for lithium ion battery applications. *RSC Adv.* **2011**, *1*, 1834–1840.
- (16) Eom, K.; Jung, J.; Lee, J. T.; Lair, V.; Joshi, T.; Lee, S. W.; Lin, Z.; Fuller, T. F. Improved stability of nano Sn electrode with high quality nano SEI formation for lithium ion battery. *Nano Energy* **2015**, *12*, 314–321.
- (17) Yang, Z.; Gewirth, A. A.; Trahey, L. Investigation of Fluoroethylene Carbonate Effects on Tin based Lithium Ion Battery Electrodes. *ACS Appl. Mater. Interfaces* **2015**, *7*, 6557–6566.
- (18) Seo, D. M.; Nguyen, C. C.; Young, B. T.; Heskett, D. R.; Woicik, J. C.; Lucht, B. L. Characterizing Solid Electrolyte Interphase on Sn Anode in Lithium Ion Battery. *J. Electrochem. Soc.* **2015**, *162*, A7091–A7095.
- (19) Paloukis, F.; Elmasides, C.; Neophytides, S. G.; Ioannides, T. Electrochemical Performance of Sn/C Nanocomposites Interphased with Varying Mixtures of Ethyl, Dimethyl and Vinylene Carbonate. *J. Electrochem. Soc.* **2016**, *163*, A1013–A1019.
- (20) Park, S.; Heon Ryu, J.; Oh, S. M. Passivating Ability of Surface Film Derived from Vinylene Carbonate on Tin Negative Electrode. *J. Electrochem. Soc.* **2011**, *158*, A498–A503.
- (21) Dalavi, S.; Guduru, P.; Lucht, B. L. Performance Enhancing Electrolyte Additives for Lithium Ion Batteries with Silicon Anodes. *J. Electrochem. Soc.* **2012**, *159*, A642–A646.
- (22) Martinez de la Hoz, J. M.; Balbuena, P. B. Reduction mechanisms of additives on Si anodes of Li ion batteries. *Phys. Chem. Chem. Phys.* **2014**, *16*, 17091–17098.
- (23) Kilibarda, G.; Schlabach, S.; Winkler, V.; Bruns, M.; Hanemann, T.; Szabó, D. V. Electrochemical performance of tin based nano composite electrodes using a vinylene carbonate containing electrolyte for Li ion cells. *J. Power Sources* **2014**, *263*, 145–153.
- (24) Szabó, D. V.; Kilibarda, G.; Schlabach, S.; Trouillet, V.; Bruns, M. Structural and chemical characterization of SnO_2 based nano particles as electrode material in Li ion batteries. *J. Mater. Sci.* **2012**, *47*, 4383–4391.
- (25) Yang, H.; Zhuang, G. V.; Ross, P. N., Jr Thermal stability of LiPF_6 salt and Li ion battery electrolytes containing LiPF_6 . *J. Power Sources* **2006**, *161*, 573–579.
- (26) Matsumoto, K.; Inoue, K.; Nakahara, K.; Yuge, R.; Noguchi, T.; Utsugi, K. Suppression of aluminum corrosion by using high concentration LiTFSI electrolyte. *J. Power Sources* **2013**, *231*, 234–238.
- (27) Dahbi, M.; Ghamous, F.; Tran Van, F.; Lemordant, D.; Anouti, M. Comparative study of EC/DMC LiTFSI and LiPF_6 electrolytes for electrochemical storage. *J. Power Sources* **2011**, *196*, 9743–9750.
- (28) Xu, K. Nonaqueous Liquid Electrolytes for Lithium Based Rechargeable Batteries. *Chem. Rev.* **2004**, *104*, 4303–4418.
- (29) Kilibarda, G.; Szabó, D. V.; Schlabach, S.; Winkler, V.; Bruns, M.; Hanemann, T. Investigation of the degradation of SnO_2 electrodes for use in Li ion cells. *J. Power Sources* **2013**, *233*, 139–147.

- (30) Park, M. S.; Wang, G. X.; Kang, Y. M.; Wexler, D.; Dou, S. X.; Liu, H. K. Preparation and Electrochemical Properties of SnO₂ Nanowires for Application in Lithium Ion Batteries. *Angew. Chem., Int. Ed.* **2007**, *46*, 750–753.
- (31) Liu, H.; Long, D.; Liu, X.; Qiao, W.; Zhan, L.; Ling, L. Facile synthesis and superior anodic performance of ultrafine SnO₂ containing nanocomposites. *Electrochim. Acta* **2009**, *54*, 5782–5788.
- (32) Parry, K. L.; Shard, A. G.; Short, R. D.; White, R. G.; Whittle, J. D.; Wright, A. ARXPS characterisation of plasma polymerised surface chemical gradients. *Surf. Interface Anal.* **2006**, *38*, 1497–1504.
- (33) Scofield, J. H. Hartree Slater subshell photoionization cross sections at 1254 and 1487 eV. *J. Electron Spectrosc. Relat. Phenom.* **1976**, *8*, 129–137.
- (34) Tanuma, S.; Powell, C. J.; Penn, D. R. Calculations of electron inelastic mean free paths. V. Data for 14 organic compounds over the 50–2000 eV range. *Surf. Interface Anal.* **1994**, *21*, 165–176.
- (35) Chen, W.; Zhu, Z.; Li, S.; Chen, C.; Yan, L. Efficient preparation of highly hydrogenated graphene and its application as a high performance anode material for lithium ion batteries. *Nanoscale* **2012**, *4*, 2124–2129.
- (36) Lee, S. Y.; Park, K. Y.; Kim, W. S.; Yoon, S.; Hong, S. H.; Kang, K.; Kim, M. Unveiling origin of additional capacity of SnO₂ anode in lithium ion batteries by realistic ex situ TEM analysis. *Nano Energy* **2016**, *19*, 234–245.
- (37) Andersson, A. M.; Abraham, D. P.; Haasch, R.; MacLaren, S.; Liu, J.; Amine, K. Surface Characterization of Electrodes from High Power Lithium Ion Batteries. *J. Electrochem. Soc.* **2002**, *149*, A1358–A1369.
- (38) Li, J. T.; Światowska, J.; Maurice, V.; Seyeux, A.; Huang, L.; Sun, S. G.; Marcus, P. XPS and ToF SIMS Study of Electrode Processes on Sn–Ni Alloy Anodes for Li Ion Batteries. *J. Phys. Chem. C* **2011**, *115*, 7012–7018.
- (39) Niehoff, P.; Passerini, S.; Winter, M. Interface Investigations of a Commercial Lithium Ion Battery Graphite Anode Material by Sputter Depth Profile X ray Photoelectron Spectroscopy. *Langmuir* **2013**, *29*, 5806–5816.
- (40) Verma, P.; Maire, P.; Novák, P. A review of the features and analyses of the solid electrolyte interphase in Li ion batteries. *Electrochim. Acta* **2010**, *55*, 6332–6341.
- (41) Winkler, V.; Hanemann, T.; Bruns, M. Comparative surface study regarding SEI features of graphite depending on the electrolyte composition. *Surf. Interface Anal.* **2016**, DOI: 10.1002/sia.6139.
- (42) El Ouatani, L.; Dedryvère, R.; Siret, C.; Biensan, P.; Reynaud, S.; Iratçabal, P.; Gonbeau, D. The Effect of Vinylene Carbonate Additive on Surface Film Formation on Both Electrodes in Li Ion Batteries. *J. Electrochem. Soc.* **2009**, *156*, A103–A113.
- (43) Etacheri, V.; Haik, O.; Goffer, Y.; Roberts, G. A.; Stefan, I. C.; Fasching, R.; Aurbach, D. Effect of Fluoroethylene Carbonate (FEC) on the Performance and Surface Chemistry of Si Nanowire Li Ion Battery Anodes. *Langmuir* **2012**, *28*, 965–976.
- (44) Nie, M.; Abraham, D. P.; Chen, Y.; Bose, A.; Lucht, B. L. Silicon Solid Electrolyte Interphase (SEI) of Lithium Ion Battery Characterized by Microscopy and Spectroscopy. *J. Phys. Chem. C* **2013**, *117*, 13403–13412.
- (45) Xu, C.; Lindgren, F.; Philippe, B.; Gorgoi, M.; Björefors, F.; Edström, K.; Gustafsson, T. Improved Performance of the Silicon Anode for Li Ion Batteries: Understanding the Surface Modification Mechanism of Fluoroethylene Carbonate as an Effective Electrolyte Additive. *Chem. Mater.* **2015**, *27*, 2591–2599.
- (46) Li, Y.; Lian, F.; Ma, L.; Liu, C.; Yang, L.; Sun, X.; Chou, K. Fluoroethylene Carbonate as Electrolyte Additive for Improving the electrochemical performances of High Capacity Li_{1.16}[Mn_{0.75}Ni_{0.25}]_{0.84}O₂ Material. *Electrochim. Acta* **2015**, *168*, 261–270.
- (47) Nie, M.; Chalasani, D.; Abraham, D. P.; Chen, Y.; Bose, A.; Lucht, B. L. Lithium Ion Battery Graphite Solid Electrolyte Interphase Revealed by Microscopy and Spectroscopy. *J. Phys. Chem. C* **2013**, *117*, 1257–1267.
- (48) Malmgren, S.; Ciosek, K.; Lindblad, R.; Plogmaker, S.; Kühn, J.; Rensmo, H.; Edström, K.; Hahlin, M. Consequences of air exposure on the lithiated graphite SEI. *Electrochim. Acta* **2013**, *105*, 83–91.

Repository KITopen

Dies ist ein Postprint/begutachtetes Manuskript.

Empfohlene Zitierung:

Winkler, V.; Kilibarda, G.; Schlabach, S.; Szabo, D. V.; Hanemann, T.; Bruns, M.
[Surface Analytical Study Regarding the Solid Electrolyte Interphase Composition of Nanoparticulate SnO₂ Anodes for Li-Ion Batteries.](#)
2016. The journal of physical chemistry <Washington, DC> / C, 120.
[doi: 10.5445/IR/1000062767](#)

Zitierung der Originalveröffentlichung:

Winkler, V.; Kilibarda, G.; Schlabach, S.; Szabo, D. V.; Hanemann, T.; Bruns, M.
[Surface Analytical Study Regarding the Solid Electrolyte Interphase Composition of Nanoparticulate SnO₂ Anodes for Li-Ion Batteries.](#)
2016. The journal of physical chemistry <Washington, DC> / C, 120 (43), 24706–24714.
[doi:10.1021/acs.jpcc.6b06662](#)